Millimeter/Submillimeter Spectroscopic Detection of Desorbed Ices: A New Technique in Laboratory Astrochemistry

Katarina M. Yocum,*,† Houston H. Smith,† Ethan W. Todd,† Leslie Mora,†

Perry A. Gerakines,‡ Stefanie N. Milam,‡ and Susanna L. Widicus Weaver†

Department of Chemistry, Emory University, Atlanta, GA, and Astrochemistry Laboratory, NASA Goddard Space Flight Center, Greenbelt, MD

E-mail: katarina.yocum@emory.edu

*To whom correspondence should be addressed

†Department of Chemistry, Emory University, Atlanta, GA

‡Astrochemistry Laboratory, NASA Goddard Space Flight Center, Greenbelt, MD

Abstract

A new laboratory technique has been developed that utilizes gas-phase, direct-absorption millimeter and submillimeter spectroscopy to detect and identify desorbed species from interstellar and cometary ice analogs. Rotational spectroscopy is a powerful structure-specific technique for detecting isomers and other species possessing the same mass that are indistinguishable with mass spectrometry. Furthermore, the resultant laboratory spectra are directly comparable to observational data from far-infrared and millimeter telescopes. Here we present the proof-of-concept measurements of the detection of thermally desorbed H_2O, D_2O, and CH_3OH originating in a solid film created at low temperature ($\sim$12 K). The surface binding energy of H_2O is reported and compared to results from traditional techniques, including mass spectrometry and quartz-crystal microbalance measurements of mass loss. Lastly, we demonstrate that this technique is capable of deriving thermodynamic values including the sublimation enthalpy and entropy of H_2O.

1. Introduction

Interstellar ice chemistry has been studied extensively through computational and laboratory studies, but after decades of research, we do not have fully-quantitative laboratory desorption data on species formed within icy dust grain mantles. The primary means of characterizing desorbed species is through mass spectrometry, and while this technique is extremely sensitive, it cannot be used to study most structural isomers or varying conformers of a given species due to mass overlaps. Many researchers use isotopic substitution to distinguish between isomers, but it has been shown that isotopologue desorption yields can differ significantly. For example, a recent laboratory study by Cruz-Diaz et al.[1] reported a higher photodesorption yield for water (H_2O) at 8 K – $(1.3\pm0.2) \times 10^{-3}$ molecules photon^{-1} – than for deuterated water (D_2O) – $(0.7\pm0.1) \times 10^{-3}$ molecules photon^{-1}. Furthermore, in the case of conformer analysis, even isotopic substitution will not be helpful in distinguishing

various product channels. Isotopic substitution coupled with mass spectrometry is the most sensitive technique for determining compositions of ices desorbed during warm-up, but it is not always optimal when studying the chemical details of the photodesorption mechanism.

An in-situ laboratory technique that is capable of probing the thermal desorption of ices is molecular rotational spectroscopy, which is structure-specific and highly sensitive. Rotational spectroscopy is the primary method used in remote observations to study species desorbed from interstellar dust grains and cometary comae. Hence, laboratory-measured rotational spectra are directly comparable to those collected via ground- and space-based telescopes at these wavelengths. Although rotational spectroscopy has less-sensitive detection limits than mass spectrometry, gas-phase rotational spectroscopic techniques complement the results of more traditional laboratory approaches to studying interstellar and cometary ice analogs (e.g., mass spectrometry, IR spectroscopy). Remarkably, despite its prolific use in molecular identification for observational astronomy, to our knowledge there are no reported laboratory spectroscopic detections of desorbed ice species in the millimeter and submillimeter (mm/submm) spectral region. This work demonstrates an experimental technique designed for analyzing desorbed species from ices using mm/submm spectroscopy. The main goals of using this technique are (1) to aid in the distinction of structural isomers that desorb from laboratory ices and (2) to produce spectroscopic results that are directly comparable to observational data from mm/submm (including far-IR) telescopes. Herein the details of the experimental design and performance are described, and the results for thermally desorbed ices composed of H_2O, D_2O, or CH_3OH are reported.

2. Background

2.1 Comparison of Laboratory Techniques

Traditional laboratory studies of interstellar ice chemistry have been conducted at IR wavelengths and are often complemented with mass spectrometry.[2–6] The IR-active vibrations

of complex molecules show significant spectral overlap due to functional groups that the molecules have in common, making unique identifications difficult without complementary mass spectrometric (MS) results. Moreover, mass spectrometers are extremely sensitive, and they can measure trace species present under ultra-high-vacuum (UHV) conditions (P $<10^{-8}$). Even so, the coupling of IR and MS cannot decipher between the isomers of molecules such as glycolaldehyde ($HCOCH_2OH$) and methyl formate ($HCOOCH_3$), both with a mass of 60 amu. This method is also unable to distinguish between something as straightforward as the methanol photodissociation products CH_3O and CH_2OH. While it is possible to perform isotopic substitutions to distinguish between photodissociation products, experiments have shown that the photodesorption yields of different isotopologues are different, as discussed above.[1] As such, the traditional technique of coupling IR spectroscopy with mass spectrometry is not sufficient to distinguish between all desorbed structural isomers of interest.

The technique presented in this work addresses this limitation of laboratory ice studies, because rotational spectroscopy is structure-specific and employs a high spectral resolution (0.1 MHz), enabling distinct identifications of each species from their unique, pure rotational spectrum, with no spectral or mass signal overlaps. Implementation of rotational spectroscopic analysis of desorbed ice species has the potential to significantly advance studies in laboratory astrochemistry and can provide a much greater understanding of the observed abundances of complex organic molecules throughout the universe.

2.2 Thermal Desorption of Water and Methanol Ices

Water is the most abundant constituent of observed interstellar and cometary ices.[7–10] Many laboratory studies of the thermal desorption of water ice have been reported and will be briefly discussed herein. Table 1 lists the kinetic parameters for the thermal desorption of water ice collected by temperature-programmed desorption (TPD) and quartz-crystal microbalance (QCM) methods as reported in previous studies. The substrate compositions,

deposition temperatures, and heating rates are also listed.

Table 1: An overview of the thermal desorption kinetic parameters of previous H_2O ice studies.

Surface Binding Energy (eV)	Desorption Order	Substrate	Deposition Temperature (K)	Heating Rate (K s^{-1})	Reference
0.48 ± 0.03	0 ± 0.25	HOPG*		0.25-2.0	Ulbricht et al.[11]
0.41 ± 0.01	0.26 ± 0.02	HOPG*	90	0.50 ± 0.01	Bolina et al.[12]
0.60 ± 0.01	0	Ru(001)	160	Isothermal	Smith et al.[13]
0.50 ± 0.01	0	Gold	10	0.02	Fraser et al.[14]
0.5 ± 0.01	0	Ru(001)/Au(111)		0.6	Speedy et al.[15]
0.45 ± 0.03	0	Graphite(0001)	85	2.5	Chakarov et al.[16]
0.45 ± 0.03		Gold coated QCM	60	0.02	Sack & Baragiola[?]
0.52	0	Sapphire		Isothermal	Haynes et al.[17]
0.44 ± 0.004	1	CsI	10	0.03	Sanford &Allamandola[?]

*Highly Oriented Pyrolytic Graphite

The surface binding energies range from 0.41 to 0.60 eV, with most values lying closer to 0.41 eV. A thorough discussion of the differences in binding energies that results from different experimental techniques can be found in the review by Burke & Brown.[18] In Section 4.2, we compare our results for H_2O using the mm/submm technique to those listed in Table 1.

Previous studies also have been performed for deuterated water (D_2O). Although the desorption processes for H_2O and D_2O are analogous, their parameters (i.e., binding energies, desorption yields) are not the same. Schmitz et al.[19] were the first to show an isotope effect in water desorption when they examined the thermal desorptions of solid H_2O and D_2O from a Ru(001) surface. Other water isotopologues have been studied, including $D_2^{18}O$[20] and $H_2^{18}O$.[13] The work presented here focuses on $D_2^{16}O$ and demonstrates our ability to detect isotopologues at their distinct frequencies.

The work presented here also includes the thermal desorption of solid CH_3OH. The thermal desorption of CH_3OH has been studied extensively[11,21–25] and an in-depth discussion of these studies can be found in the review by Burke & Brown.[18] Methanol is significant because it is one of the most abundant species in interstellar ices and is the chemical starting point for many larger complex organic molecules in interstellar and cometary chemistry.

The current effort focuses on benchmarking experiments on the thermal desorption of water, given the extensive amount of existing literature related to H_2O desorption available

for comparison. Measurements were also extended to include studies of solid D_2O and CH_3OH to provide a more complete proof-of-concept.

3. Experimental

3.1 Ice Chamber Description

The experiment was designed to combine a traditional laboratory ice analog setup with a millimeter/submillimeter spectrometer in order to study gas species thermally desorbed from ice films. A schematic of the experimental setup is shown in Figure 1.

The vacuum chamber has six 8-inch ConFlat® (CF) ports. The bottom port is attached to a turbo molecular pump (Œrlikon Leybold TW90) which achieves a chamber pressure of 1×10^{-9} Torr. The set-up also includes a mm/submm spectrometer (output frequency ranges of 75-1000 GHz, 1.8-1.9 THz, and 2.5-2.6 THz), a cryostat, a residual gas analyzer (Stanford Research Systems, Model RGA300), a UV photolysis lamp, a 670-nm laser diode, and a fine-control gas dosing valve. The cryostat takes up another of the six CF ports, while the remaining four are connected to multi-port flanges. The left, right, and front multi-port flanges have three 2.75-inch CFs, and the top flange has four 2.75-inch CFs.

A polished gold sample substrate (Advanced Research Systems, Inc., SHNO-1B) is held at the center of the chamber by the cold arm of a closed-cycle helium cryostat (APD Cryogenics 256844D1, Expander Model DE-202B) connected to a helium compressor (APD Cryogenics, Model HC-2). The temperature of the substrate is varied using a temperature controller (Scientific Instruments, Model 9700) that monitors the temperature with a silicon diode sensor (Scientific Instruments, Model SI-410). The cryostat achieves a base temperature of 12 K at the substrate holder. A 36-Ω metallized heater (Advanced Research Systems, Inc.) is located near the tip of the cold finger and can heat the gold substrate to 200 K. Ices may be photolyzed by a static microwave-discharge hydrogen lamp (Opthos Instrument Company, LLC) that is filled with 10% H_2 and 90% Ar and emits primarily Lyman-α photons (λ =

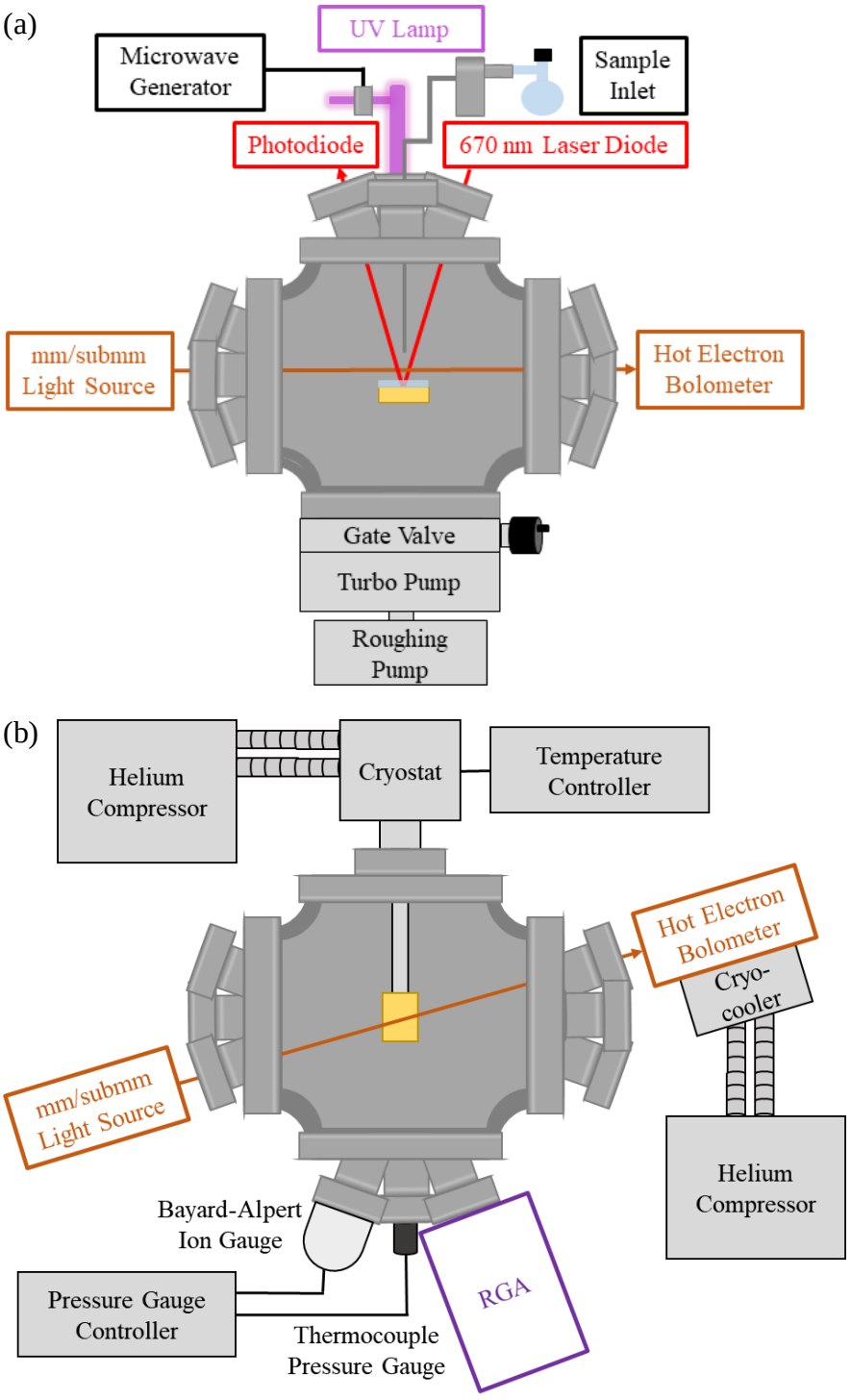

Figure 1: Schematics of the (a) side and (b) top views of the experimental setup.

121.6 nm). The hydrogen mixture is excited by a discharge, which is sustained by an Evenson cavity connected to a microwave generator (Opthos Instrument Company, LLC). The UV photons enter the chamber through a MgF_2 window located on the top of the chamber and are directed at the gold substrate.

In the present work, the gas-phase products of thermally desorbed ices are detected using the mm/submm spectrometer similar to one described previously.[26] A detailed schematic of the mm/submm spectrometer is shown in Figure 2. First, microwave radiation (0.000250-50 GHz) is generated by an analog signal generator (Agilent Technologies E8257D PSG). The radiation travels to a mm-wave multiplier (Virginia Diodes Inc. WR10) and is multiplied to the range of 75-110 GHz. Higher frequencies from 110 GHz to 1 THz are achieved by combinations of frequency multipliers that connect to the output of the mm-wave multiplier. A Teflon lens (Thorlabs^{TM}) collimates the light, and then it enters the chamber through a sapphire view-port. The mm/submm light passes ∼1-2 cm above the ice, exits the chamber through a second sapphire viewport, and is focused via a second Teflon lens onto the cryo-cooled THz bolometer (QMC Instruments QNbB/PTC). Lastly, a lock-in amplifier (Stanford Research SR830 DSP) is used to increase the signal-to-noise ratio. The input radiation is frequency-modulated at 0.2 kHz and the lock-in is used for phase-sensitive detection, resulting in second-derivative line shapes. Spectra are recorded with a resolution of 0.10 MHz. The number of spectral averages varies, based on experimental conditions (i.e. low concentration species could require up to 1000 averages or more, but higher concentration or highly absorbing species require as few as 10 averages). The spectrometer is controlled using custom design data acquisition software.

The all-metal gas dosing valve (Pfeiffer Vacuum Inc., Model UDV 046), located on the top 4-port CF, slowly introduces gas into the chamber through a small capillary tube directed at the 12-K gold substrate, where it condenses to form an ice film. The ice thickness and deposition rate is monitored by the 670-nm laser. The 670-nm laser diode (Thorlabs^{TM}, Model CPS670F) is located on the top port of the chamber. The light enters through a

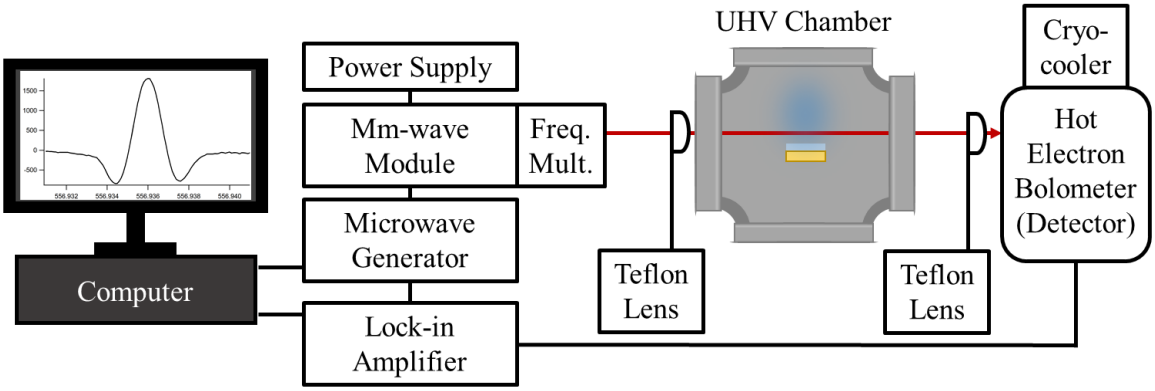

Figure 2: Schematic of the mm/submm spectrometer comprised of a microwave generator, mm-wave multiplier, frequency multipliers (Schottky diodes), lock-in amplifier, and a hot electron bolometer.

fused silica window, with an incidence angle of 29.4° from normal to the substrate. The light beam reflects from the gold substrate, passes through a second fused-silica window, and is detected by a photodiode (Thorlabs^{TM}, Model DET100A). As the ice becomes thicker, the detected laser intensity oscillates due to constructive and destructive interference from the refracted and reflected light beams. The measured voltage creates an interference fringe pattern which is used to calculate the ice thickness using the Bragg equation (Tempelmeyer & Mills 1968 and references therein[27]):

$$d = \frac{m\lambda}{2\sqrt{n^2 - sin^2\theta}}, \tag{1}$$

where m is the number of oscillations, λ is the laser wavelength (670 nm), n is the real part of the refractive index, and θ is the incidence angle of the laser (29.4°).

3.2 Methods

3.2.1 Submm Limit of Detection

The limit of detection (LOD) is defined as the lowest gas density at which the spectrometer can detect specific rotational transitions with a signal-to-noise ratio (SNR) of at least three,

therefore the LOD depends on the intensity of the specific transition probed. In general, when determining the LOD for different analytes, five rotational transitions were tested by slowly increasing the analyte partial pressure using the high-precision gas dosing valve and collecting mm/submm spectra at each pressure. The rotational transition with the lowest SNR out of the five was used to determine the LOD. Knowing the LOD is important for calculating the plausibility of detecting different species when performing thermal and/or photon-induced desorption experiments.

3.2.2 Thermal Desorption of Ices

The experimental procedure for studying thermal desorption using this experiment is analogous to a traditional TPD experiment, but with one difference: the desorbed species are detected using mm/submm spectroscopy instead of mass spectrometry.

The ices were formed at 12 K as described above, by slowly introducing a vapor into the chamber at $\sim 5 \times 10^{-7}$ Torr. The vapor entered the chamber about 1 inch above the gold substrate through a capillary tube connected to the high-precision gas dosing valve. Next, the ices were heated from 12-200 K at a 1 K min^{-1} rate and the rotational absorption signal of the thermally-desorbed species was recorded as a function of time.

4. Results and Discussion

4.1 Submm Detection Limits of H_2O, D_2O, and CH_3OH

The gas-phase limit of detection (LOD) was determined for H_2O, D_2O, and CH_3OH using the procedure described in Section 3.2.1. The LOD of the $1_{1,0} \leftarrow 1_{0,1}$ rotational transition of H_2O was determined by slowly increasing pressure in the chamber through the gas dosing valve. The pressure of water was increased in 1×10^{-8} Torr increments, and the spectrum of the $1_{1,0} \leftarrow 1_{0,1}$ rotational transition was collected at each step. Once a SNR of 3 or higher was achieved, the corresponding pressure of water (as measured by the RGA) was converted to

a density using the ideal gas law. The same procedure was performed for D_2O and CH_3OH by detecting the $1_{1,1} \leftarrow 0_{0,0}$ and $13_{-1,13} \leftarrow 12_{-1,12}$ transitions, respectively. The LODs for all three analytes are listed in Table 2.

Table 2: mm/submm spectroscopic limit of detection of H_2O, D_2O, and CH_3OH

Analyte	LOD (molecules cm^{-3})	Frequency (MHz)	# of scans averaged	SNR
H_2O	1.1×10^9	556935.99	30	5.6
D_2O	1.7×10^9	607349.44	30	3.8
CH_3OH	3.1×10^{10}	627170.48	30	8.3

The LOD of H_2O was the lowest for all three species followed by D_2O and CH_3OH, respectively. While the detection limits of submm spectroscopy demonstrated here are extremely low, they are still more than an order of magnitude higher than those determined when mass spectrometry is used (10^8 molecules cm^{-3}).[28] For a true comparison the data collection time must be noted for both techniques. For the current experiment, it takes 3.5 minutes to collect 30 spectral averages at a 0.1 MHz resolution over a 10 MHz spectral bandwidth. This was the case for all three submm LOD measurements reported. Mass spectrometric measurements take a matter of seconds to achieve a detection limit of 10^8 molecules cm^{-3}. The submm LOD could be lowered by averaging more scans, but this would increase the data collection time to the point where it would not be practical for most studies (i.e., >24 hours). Nonetheless, for molecules with similar line strengths and densities to those reported in Table 2, detection using this technique is sufficient.

4.2 Thermal Desorption of H_2O, D_2O, and CH_3OH

Figure 3 shows the submm spectra for thermally desorbed H_2O, D_2O, and CH_3OH.

Thermal desorption traces of desorption rate vs. temperature were constructed for H_2O from the measured peak absorptions (see Figures 5 and 6). Thermal desorption traces for three different ice thicknesses are shown in Figure 5. These spectra were collected from 100 – 200 K at 5 K increments. A relative thermal desorption rate was obtained from the peak absorption of each rotational transition at a given temperature by the following method.

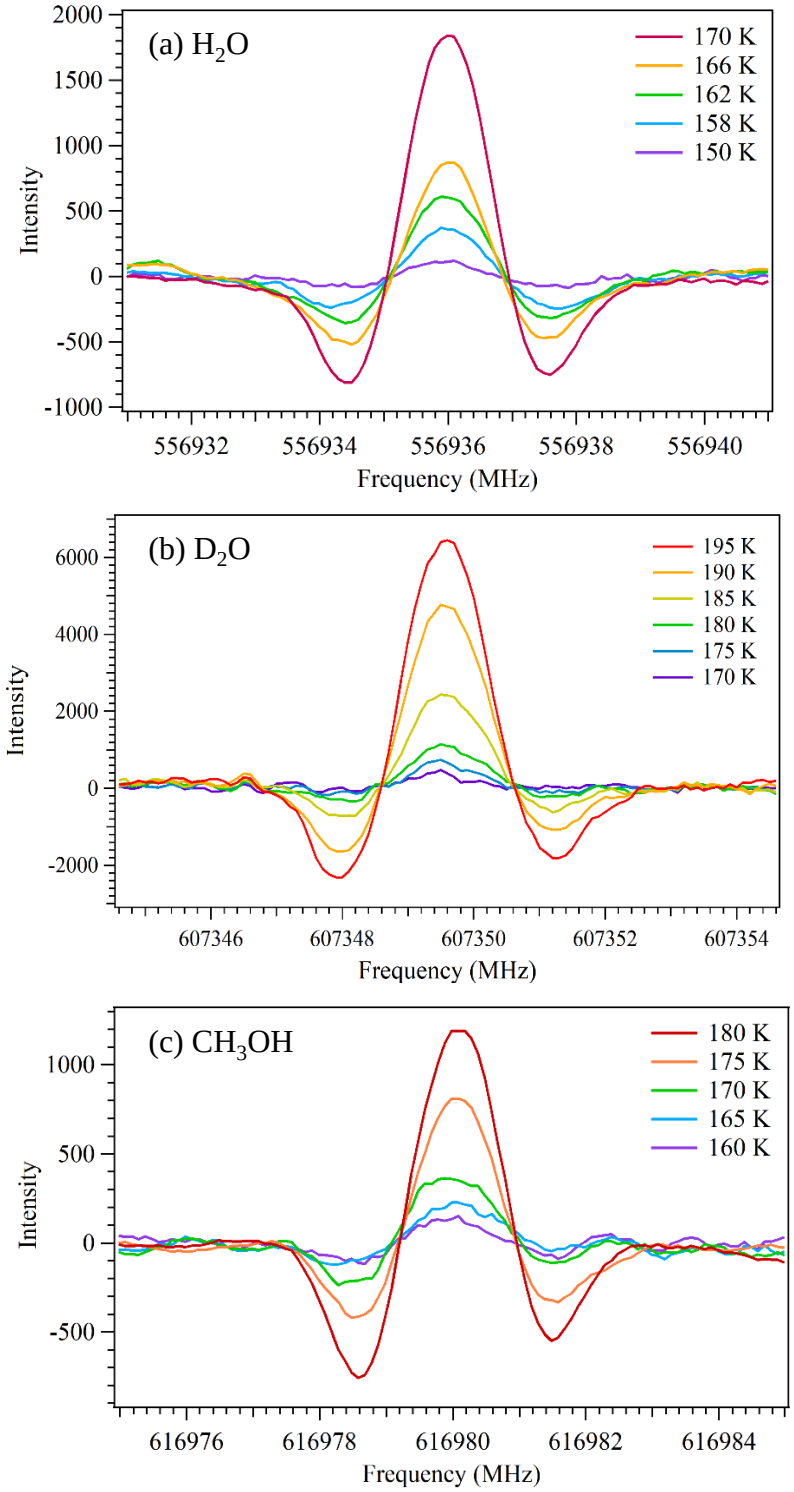

Figure 3: (a) Spectra of the $1_{1,0} \leftarrow 1_{0,1}$ rotational transition of thermally desorbed H_2O at 150-170 K. (b) Spectra of the $1_{1,1} \leftarrow 0_{0,0}$ rotational transition of thermally desorbed D_2O at 170-195 K. (c) Spectra of the $13_{-1,13} \leftarrow 12_{-1,12}$ rotational transition of thermally desorbed CH_3OH at 160-180 K.

The peak intensity, $I(T)$, of the rotational transition is directly proportional to the thermal desorption rate, R, and the loss of ice molecules over time, $-\frac{dN}{dt}$:

$$I(T) \propto R \propto -\frac{dN}{dt} \tag{2}$$

and

$$-\frac{dN}{dt} = NAexp(\frac{-E_{des}}{k_B T}) \tag{3}$$

where N is the number of molecules in the ice, A is the pre-exponential factor, E_{des} is the ice surface binding energy, k_B is the Boltzmann constant, T is the temperature in Kelvin, and a first-order desorption process was assumed. By plotting the relative thermal desorption rate obtained from the peak absorption signal versus inverse temperature, E_{des} can be calculated from an exponential fit (see Figure 7).

To verify the linear proportionality between absorption intensity, $I(T)$, and desorption rate, R, (Eq. 2), a quantitative thermal desorption rate was determined by isothermally desorbing 1.6 μm thick H_2O ices at 150, 155, 162, 165, 168, and 170 K. Interference fringes were measured using the 670-nm laser diode. The thermal desorption rate at each temperature was calculated in μm s^{-1}. The submm absorption intensities at these temperatures were then plotted against the μm s^{-1} desorption rates (see Figure 4). A linear best fit gave the calibration equation

$$I(T) = 1.264 \times 10^6(R) + 126.5 \tag{4}$$

and an R^2 of 0.99.

For this new technique, it may be more useful to calibrate the thermal desorption rate with respect to the number density of the desorbed gas-phase species. For this calibration, the density of H_2O molecules was measured using the RGA from 150 – 180 K. This calibration corrects for the effective pumping speed (EPS) of the chamber and the gas-phase species that

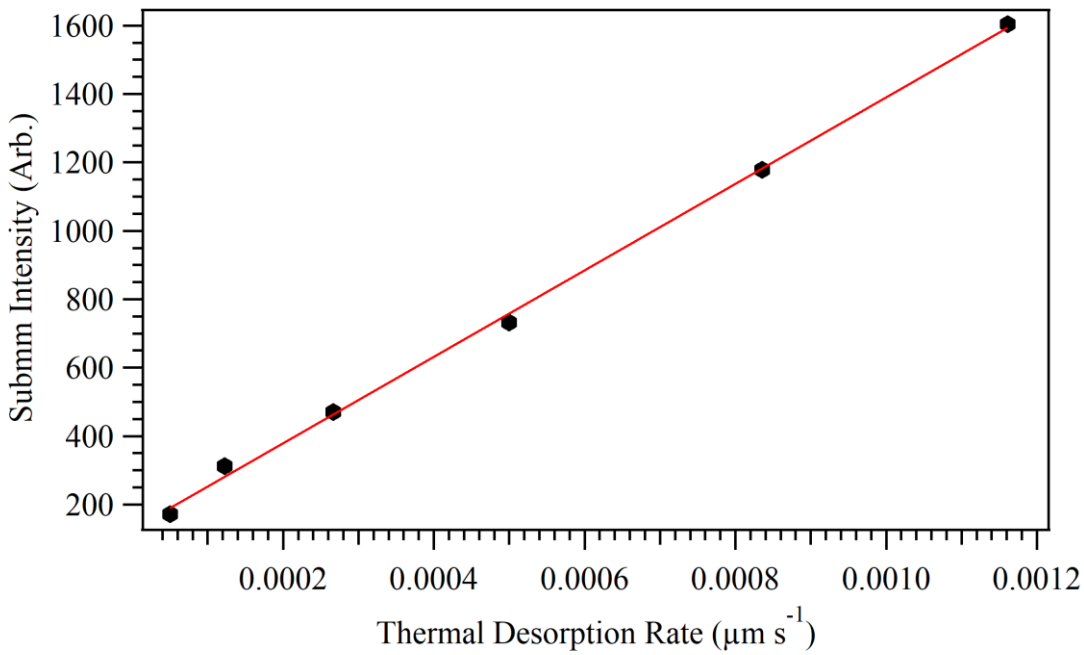

Figure 4: Linear relationship between the submm peak absorption intensity and the thermal desorption rate of a H_2O ice. The 1-σ error bars are not visible on this plot.

recondense onto the cryostat. First, the density of H_2O (molecules cm^{-3}) was multiplied by the EPS (cm^3 s^{-1}) and divided by the volume of the chamber (cm^3). Next, the rate of which the cryostat removes H_2O from the chamber was added to the EPS calibrated thermal desorption rate (molecules cm^{-3} s^{-1}). The rate of which molecules condense onto the cryostat was measured by simply introducing a known density of H_2O vapor into the chamber with the gate valve closed, and the density of H_2O was measured over time with the RGA. These measurements were performed across the thermal desorption window of H_2O ice (145-180 K). The recondensation rate was the same across this temperature range. The submm absorption intensity, $I(T)$, was then plotted against R in molecules cm^{-3} s^{-1} to determine the desorption rate calibration function

$$I(T) = 3.04 \times 10^{-9}(R) - 4.37, \tag{5}$$

and a R^2 value of 0.99. The calibrations reported in Eq. 4 and 5 are necessary for future reports of quantitative values of desorbed species (e.g. gas-phase concentrations).

Since this is the first report of detecting thermally desorbed ices spectroscopically, no previously reported studies offered a direct comparison. The spectroscopic method used here differs from TPD experiments simply because it monitors the center frequency of a rotational transition instead of a mass signal. Nonetheless, the data were analyzed in a similar manner as TPD data to determine E_{des}. The binding energy reported here for water matched those reported by several others within experimental error (see Table 1).[11,14–17,29]

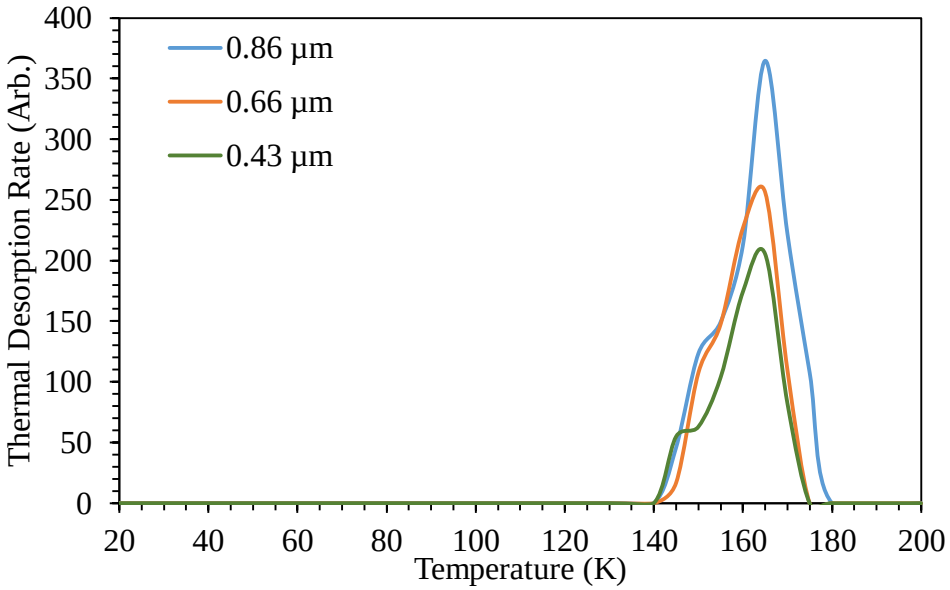

Figure 5: Thermal desorption curve of 0.86, 0.66, and 0.43 μm thick H_2O ices.

In Figure 5 the thermal desorption curves of the 0.86, 0.66, and 0.43 μm thick ices all peak at the same temperature, 165 K, suggesting first-order kinetics.[14] However, it has been shown that fractional-order kinetics better describes hydrogen-bonded systems including water[12,30] and alcohols including methanol and ethanol.[21,23,31] Furthermore, a study by Green et al.[22] showed that at low methanol coverages, thermal desorption demonstrates fractional order, and at high coverages the desorption follows zero-order kinetics. Here the desorption order was not quantitatively determined because the ice coverage was not well-quantified.

The thermal desorption curve of a thicker ice, 1.6 μm, is shown in Figure 6. The thermal desorption curve shown in Figure 6 was produced using the same procedure as mentioned previously by monitoring the intensity of the $1_{1,0} \leftarrow 1_{0,1}$ rotational transition of thermally

desorbed H_2O over time as the ice was heated from 12-190 K at a 1 K min^{-1} rate. The mass signal at 18 amu was simultaneously monitored by the RGA.

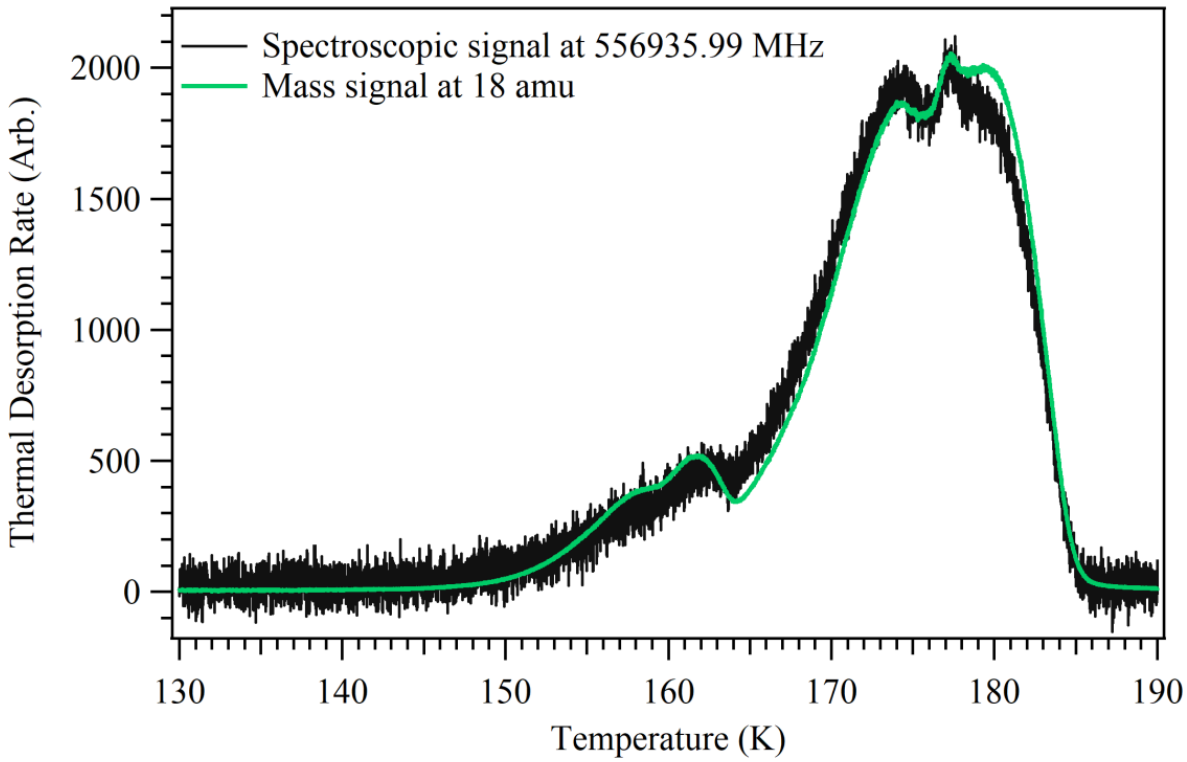

Figure 6: Thermal desorption curve of a 1.6 μm thick H_2O ice detected with the mm/submm spectrometer (black) and the RGA (green). The mass signal was multiplied by 10^{10} to be scaled to the intensity of the spectroscopic signal.

There are three noticeable features that appear in the thermal desorption curve in Figure 6 at ~160, 173, and 178 K. These features result from phase changes of the water ice. A peak at ~150-160 K has been reported several times in the literature as being present in water thermal desorption curves and corresponds to the phase change from amorphous solid water to cubic crystalline ice.[12,15,30,32,33] A higher temperature phase transition at 175 K from cubic crystalline ice to hexagonal ice was seen in the desorption trace of the 0.86 μm thick ice in Figure 5 and at ~178 K in the 1.6 μm thick ice in Figure 6. Bolina et al.[12] were the first to observe this phase transition in their TPD from HOPG studies. By 180-185 K, the 1.6 μm thick ice was completely sublimated. Figure 6 also displays a comparison to a thermal desorption curve detected by the RGA at 18 amu. The peak thermal desorption rates, phase

transitions, and final and initial detections occur at the same temperatures in both curves. Therefore, measuring thermally desorbed species with mm/submm spectroscopy is directly comparable to the well-established mass spectrometric TPD method.

Furthermore, the surface binding energy (E_{des}) was calculated by plotting the relative thermal desorption rate versus inverse temperature. The exponential fit to these data yielded E_{des} (see Figure 7).

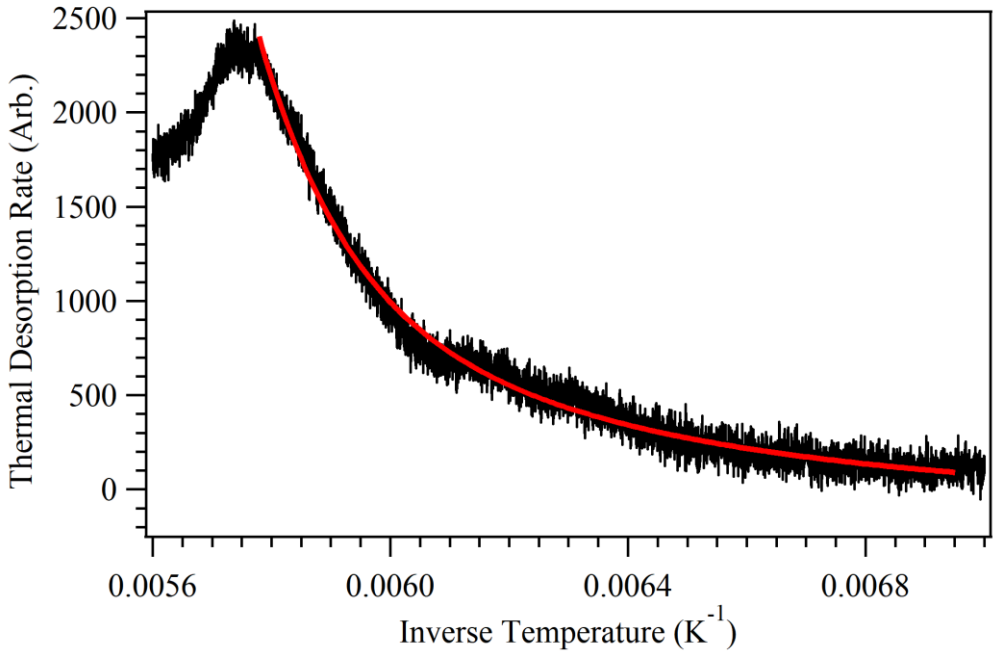

Figure 7: Thermal desorption rate versus inverse temperature for the 1.6 μm thick H_2O ice. The exponential fit to determine E_{des} is shown in red.

The binding energy calculated from the exponential fit in Figure 7 was 0.45 ± 0.06 eV. The average binding energy after repeating this experiment five times was 0.47 ± 0.02 eV.

This new technique can also be used to determine the sublimation enthalpy, ΔH, of different ices over specific temperature ranges using the Clausius-Clapyron equation

$$P_V = e^{\frac{-\Delta G}{RT}}. \tag{6}$$

In Eq. 6 P_V is vapor pressure, ΔG is the free energy of sublimation, R is the ideal gas constant, T is temperature, and

$$\Delta G = \Delta H - T\Delta S, \tag{7}$$

where ΔH is the sublimation enthalpy and ΔS is the sublimation entropy. Rearrangement of Eq. 6 gives the linear form of the Clausius-Clapyron equation

$$ln(P_V) = -\frac{\Delta H}{RT} + \frac{\Delta S}{R}, \tag{8}$$

By plotting $ln(P_V)$ versus $1/T$ the sublimation enthalpy can be obtained from the slope, and the entropy from the y-intercept of the best fit line (see Figure 8). The Knudsen equation was used to derive the vapor pressure for temperatures of 145-175 K:

$$R = \frac{P_V}{\sqrt{2\pi M k_B T}}, \tag{9}$$

where R is the desorption rate and M is molecular mass. The linear fit in Figure 8 had an R^2 value of 0.99 and the sublimation enthalpy and entropy were 0.286 $\pm$ 0.006 eV and 0.00127 $\pm$ 0.00004 eV K^{-1}, respectively.

Although the results using this new technique matched literature values within experimental error, the detection limits of mass spectrometry are lower than submm spectroscopy. Therefore, using this technique for determining kinetic parameters is not recommended over mass spectrometry unless one is studying species of the same mass which cannot be distinguished. Nonetheless, the agreement between the two techniques shows that the new method provides a valuable path forward for studying interstellar and cometary ice chemistry when infrared and mass spectrometric analysis does not provide sufficient means for identifying products.

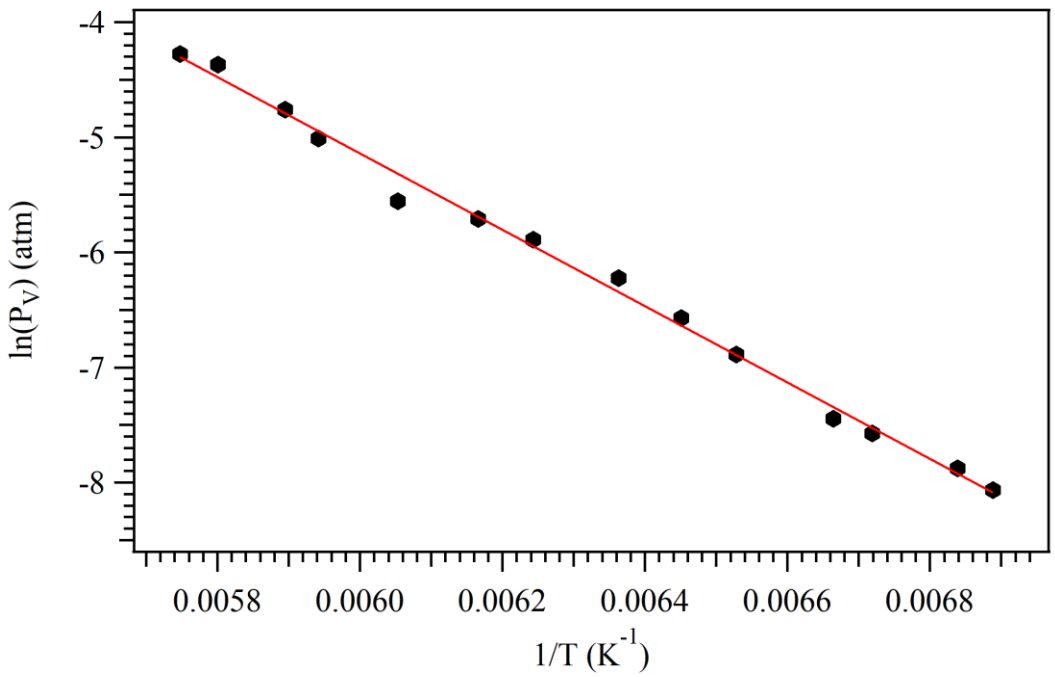

Figure 8: Clausius-Clayron relationship for a 1.6 μm thick H_2O ice from 145-175 K to determine ΔH and ΔS. The 1-σ error bars are not visible on this plot.

5. Conclusions and Future Work

This study presents a new laboratory technique for detecting thermally desorbed ices. This is the first known report of detecting desorbed species from laboratory ices spectroscopically at mm/submm wavelengths. This technique is powerful in that it is capable of distinguishing isomeric products that may form during desorption of ices, and the submm spectra are directly comparable to observational data from far-infrared and millimeter observatories. This work has shown proof-of-concept for analyzing thermally desorbed ices with mm/submm spectroscopy by presenting submm spectra of thermally desorbed H_2O, D_2O, and CH_3OH ices. Efforts are currently underway for optimizing the detection of photodesorbed H_2O and CH_3OH ices and their photoproducts. The focus for these future experiments will be on the detection of the photodesorbed OH radical.

Acknowledgement

This work was supported through NASA's Astrophysics Research and Analysis Program (NNH17ZDA001N, 17-APRA17-0030). Additional support was provided by the Planetary Science Division Internal Scientist Funding Program through the Fundamental Laboratory Research (FLaRe) work package. The authors thank Danna Qasim and AJ Mesko for their work on previous iterations of the experimental design; Dr. Jay (Alec) Kroll and Ayanna Jones for their assistance over the last few months of data collection; and Connor Wright, Hayley Bunn, Kevin Roenitz, Dr. Luyao Zou, and Dr. James P. McMillian for their support and assistance. The authors gratefully acknowledge the loan of original test equipment from Dr. Reggie Hudson, Dr. Thomas Orlando, and Dr. Michael Heaven, without which the experimental design could not have been tested.

References

(1) Cruz-Diaz, G. A.; Martn-Domnech, R.; Moreno, E.; Muoz Caro, G. M.; Chen, Y.-J. New measurements on water ice photodesorption and product formation under ultraviolet irradiation. *Mon. Not. R. Astron. Soc.* **2017**, *474*, 3080–3089.

(2) Greenberg, J.; Yencha, A.; Corbett, J.; Frisch, H. Ultraviolet effects on the chemical composition and optical properties of interstellar grains. *Mem. Soc. Roy. Sciences Liege* **1972**, *6e serie*, 425–436.

(3) Allamandola, L.; Sandford, S.; Valero, G. Photochemical and thermal evolution of interstellar/precometary ice analogs. *Icarus* **1988**, *76*, 225–252.

(4) Hudson, R.; Donn, B. An experimental study of the sublimation of water ice and the release of trapped gases. *Icarus* **1991**, *94*, 326–332.

(5) Öberg, K. I.; Linnartz, H.; Visser, R.; van Dishoeck, E. F. Photodesorption of Ices. II. H_2O and D_2O. *Astrophys. J.* **2009**, *693*, 1209–1218.

(6) Abplanalp, M. J.; Gbi, S.; Kaiser, R. I. On the formation and the isomer specific detection of methylacetylene (CH_3CCH), propene (CH_3CHCH_2), cyclopropane (c-C_3H_6), vinylacetylene (CH_2CHCCH), and 1,3-butadiene ($CH_2CHCHCH_2$) from interstellar methane ice analogues. *Phys. Chem. Chem. Phys.* **2019**, *21*, 5378–5393.

(7) Gibb, E. L.; Whittet, D. C. B.; Boogert, A. C. A.; Tielens, A. G. G. M. Interstellar ice: The Infrared Space Observatory legacy. *Astrophys. J., Suppl. Ser.* **2004**, *151*, 35–73.

(8) Lecacheux, A.; Biver, N.; Crovisier, J.; Bockelée-Morvan, D.; Baron, P.; Booth, R. S.; Encrenaz, P.; Florén, H.-G.; Frisk, U.; Hjalmarson, A. et al. Observations of water in comets with Odin. *Astron. Astrophys.* **2003**, *402*, L55–L58.

(9) Öberg, K. I.; Boogert, A. C. A.; Pontoppidan, K. M.; van den Broek, S.; van Dishoeck, E. F.; Bottinelli, S.; Blake, G. A.; Evans, N. J. The Spitzer ice legacy: Ice evolution from cores to protostars. *Astrophys. J.* **2011**, *740*, 109.

(10) Boogert, A. A.; Gerakines, P. A.; Whittet, D. C. Observations of the icy universe. *Ann. Rev. Astron. Astrophys.* **2015**, *53*, 541–581.

(11) Ulbricht, H.; Zacharia, R.; Cindir, N.; Hertel, T. Thermal desorption of gases and solvents from graphite and carbon nanotube surfaces. *Carbon* **2006**, *44*, 2931–2942.

(12) Bolina, A. S.; Wolff, A. J.; Brown, W. A. Reflection absorption infrared spectroscopy and temperature-programmed desorption studies of the adsorption and desorption of amorphous and crystalline water on a graphite surface. *J. Phys. Chem. B* **2005**, *109*, 16836–16845, PMID: 16853142.

(13) Smith, J. A.; Livingston, F. E.; George, S. M. Isothermal desorption kinetics of crystalline H_2O, $H_2^{18}O$, and D_2O ice multilayers. *J. Phys. Chem. B* **2003**, *107*, 3871–3877.

(14) Fraser, H. J.; Collings, M. P.; McCoustra, M. R. S.; Williams, D. A. Thermal desorption

of water ice in the interstellar medium. *Mon. Not. R. Astron. Soc.* **2001**, *327*, 1165–1172.

(15) Speedy, R. J.; Debenedetti, P. G.; Smith, R. S.; Huang, C.; Kay, B. D. The evaporation rate, free energy, and entropy of amorphous water at 150 K. *J. Chem. Phys.* **1996**, *105*, 240–244.

(16) Chakarov, D.; Österlund, L.; Kasemo, B. Water adsorption on graphite (0001). *Vacuum* **1995**, *46*, 1109–1112.

(17) Haynes, D. R.; Tro, N. J.; George, S. M. Condensation and evaporation of water on ice surfaces. *J. Phys. Chem.* **1992**, *96*, 8502–8509.

(18) Burke, D. J.; Brown, W. A. Ice in space: surface science investigations of the thermal desorption of model interstellar ices on dust grain analogue surfaces. *Phys. Chem. Chem. Phys.* **2010**, *12*, 5947–5969.

(19) Schmitz, P.; Polta, J.; Chang, S.-L.; Thiel, P. Isotope effect in water desorption from Ru(001). *Surf. Sci.* **1987**, *186*, 219–231.

(20) Chaix, L.; van den Bergh, H.; Rossi, M. J. Real-time kinetic measurements of the condensation and evaporation of D_2O molecules on ice at 140 K >T>220 K. *J. Phys. Chem. A* **1998**, *102*, 10300–10309.

(21) Bolina, A. S.; Wolff, A. J.; Brown, W. A. Reflection absorption infrared spectroscopy and temperature programmed desorption investigations of the interaction of methanol with a graphite surface. *J. Chem. Phys.* **2005**, *122*, 044713.

(22) Green, S. D.; Bolina, A. S.; Chen, R.; Collings, M. P.; Brown, W. A.; McCoustra, M. R. S. Applying laboratory thermal desorption data in an interstellar context: sublimation of methanol thin films. *Mon. Not. R. Astron. Soc.* **2009**, *398*, 357–367.

(23) Nishimura, S. Y.; Gibbons, R. F.; Tro, N. J. Desorption kinetics of methanol from Al_2O_3(0001) studied using temperature-programmed desorption and isothermal desorption. *J. Phys. Chem. B* **1998**, *102*, 6831–6834.

(24) Sandford, S. A.; Allamandola, L. J. Condensation and vaporization studies of CH_3OH and NH_3 ices: Major implications for astrochemistry. *Astrophys. J.* **1993**, *417*, 815–825.

(25) Wolff, A. J.; Carlstedt, C.; Brown, W. A. Studies of binary layered CH_3OH/H_2O ices adsorbed on a graphite surface. *J. Phys. Chem. C* **2007**, *111*, 5990–5999.

(26) Carroll, P. B.; Drouin, B. J.; Weaver, S. L. W. The submillimeter spectrum of glycoaldehyde. *Astrophys. J.* **2010**, *723*, 845–849.

(27) Tempelmeyer, K. E.; Mills, D. W. Refractive index of carbon dioxide cryodeposit. *J. Appl. Phys.* **1968**, *39*, 2968–2969.

(28) Eckel-passow, J. E.; Oberg, A. L.; Therneau, T. M.; Bergen, I., H. R. An insight into high-resolution mass-spectrometry data. *Biostatistics* **2009**, *10*, 481–500.

(29) Sack, N. J.; Baragiola, R. A. Sublimation of vapor-deposited water ice below 170 K, and its dependence on growth conditions. *Phys. Rev. B* **1993**, *48*, 9973–9978.

(30) Smith, R. S.; Huang, C.; Wong, E.; Kay, B. D. Desorption and crystallization kinetics in nanoscale thin films of amorphous water ice. *Surf. Sci.* **1996**, *367*, L13–L18.

(31) Wu, M. C.; Truong, C. M.; Goodman, D. W. Interactions of alcohols with a nickel oxide(100) surface studied by high-resolution electron energy loss spectroscopy and temperature-programmed desorption spectroscopy. *J. Phys. Chem.* **1993**, *97*, 9425–9433.

(32) Dohnálek, Z.; Ciolli, R. L.; Kimmel, G. A.; Stevenson, K. P.; Smith, R. S.; Kay, B. D. Substrate induced crystallization of amorphous solid water at low temperatures. *J. Chem. Phys.* **1999**, *110*, 5489–5492.

(33) Smith, R. S.; Kay, B. D. Molecular beam studies of kinetic processes in nanoscale water films. *Surf. Rev. Lett.* **1997**, *04*, 781–797.

Graphical TOC Entry

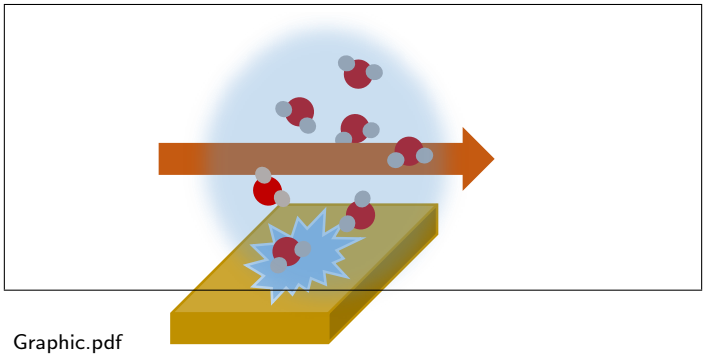

Graphic.pdf